JOURNAL OF GEOPHYSICAL RESEARCH, VOL. 98, NO. A4, PAGES 5865–5879, APRIL 1, 1993

DE 1 Particle and Wave Observations in Auroral Kilometric Radiation (AKR) Source Regions

J. D. MENIETTI[1] AND J. L. BURCH

Department of Space Sciences, Southwest Research Institute, San Antonio, Texas

R. M. WINGLEE

Department of Geophysics, University of Washington, Seattle

D. A. GURNETT

Department of Physics and Astronomy, University of Iowa, Iowa City

The high-altitude plasma instrument on board the DE 1 satellite was operating during several near crossings of the auroral kilometric radiation (AKR) source in the nightside auroral region. Observations of electron distributions indicate a region of perpendicular heating ($T_\perp/T_\parallel > 10$) adjacent to and within the source region. Loss cones, trapped particles, beams, and electron conical distributions are also observed near and within the source region, which extends perpendicular to the magnetic field line for at least 20 km. Near the AKR source region wave-particle interactions appear to have modified the observed electron distributions. We compare the observations to those predicted by recently published numerical simulations.

INTRODUCTION

The theory of the cyclotron maser instability has had much success in explaining observations of auroral kilometric radiation (AKR) to date. *Wu and Lee* [1979] have demonstrated that a loss cone distribution of electrons within a region of depleted plasma density (with ratio of plasma frequency to gyrofrequency $f_p/f_g < 0.3$) can be an effective free energy source for the generation of auroral kilometric radiation. This distribution provides the requirement of the cyclotron maser instability (CMI) that $df/dv_\perp > 0$. As pointed out by *Omidi and Gurnett* [1982] and *Omidi et al.* [1984], in addition to the loss cone, the "hole" distribution and the "bump" or trapped particle distribution can also act as free-energy sources of AKR. *Dusenbury and Lyons* [1982], *LeQueau et al.* [1984], and *Lin et al.* [1986] have also shown that the hole distribution can be significant under certain conditions in the generation of AKR. *Louarn et al.* [1990] have shown that the trapped electron population may also be an effective free-energy source.

The AKR source region is associated with inverted V events [*Gurnett*, 1974; *Green et al.*, 1979; *Benson and Calvert*, 1979]. *Sharp et al.* [1979] have indicated that energetic upward flowing ion beams observed in association with inverted V events may be due to parallel electric fields beneath the satellite. Such electric fields are hypothesized as the source of the inverted V events and are believed to play an important role in the generation of AKR [*Wu et al.*, 1982; *Wu*, 1985]. *Benson and Calvert* [1979] have shown that AKR has a low-frequency cutoff at the R-X cutoff, which for a low-density plasma is very near the electron gyrofrequency.

To date, no satellite has been capable of obtaining a complete distribution in phase space on a time scale adequate to resolve the question of the most effective free-energy source of AKR. Typically the best satellites require several seconds to obtain a complete distribution in phase space. During this time, within an AKR source region the waves would have grown and already altered the existing plasma distribution.

Observations of distributions in the AKR source region have recently been reported by investigators of the Viking satellite data. *Ungstrup et al.* [1990] have reported wide loss cones adjacent to the AKR source region, but field-aligned potentials and nearly filled loss cones appear within the source region. *Ungstrup et al.* [1990] attribute the filling of the loss cone to the AKR instability and fast diffusion of electrons as predicted by the cyclotron maser theory [*Wu et al.*, 1982]. *Louarn et al.* [1990] have reported simultaneous measurements of electromagnetic (EM) fields and particle distributions measured by the Viking satellite during a crossing of the AKR source region. They have determined that trapped electrons may play an important role in the generation of AKR. *Hilgers* [1992] have subsequently shown that density cavities of dimensions < 20 km are associated with AKR sources and that AKR seems to exist in regions where the ratio of energetic to thermal electron number densities is greater than 0.3 and $f_p/f_g < 0.15$. During 1981, DE 1 flew through the nightside auroral region at altitudes > 8000 km, a region that is believed to be at the upper extent of the source region of AKR. We here report DE 1 particle and wave data for passes of the nightside auroral region near the AKR source center. We will compare

[1]Now at the Department of Physics and Astronomy, University of Iowa, Iowa City.

Paper number 92JA02340.
0148-0227/93/92JA-02340$05.00

these results to those reported by Viking and also to recent numerical simulation studies of *Winglee and Pritchett* [1986] which show a great similarity to the observations.

OBSERVATIONS

The high-altitude plasma instrument (HAPI) and the plasma wave instrument (PWI) have been described by many authors and will not be discussed here [cf. *Burch et al.*, 1981; *Shawhan et al.*, 1981]. In Plate 1 we show an energy versus time spectrogram with energy flux color coded according to the color bar at the right. The pass is of the nightside auroral region on October 12, 1981 (day 285). Precipitating electrons are shown in the top panel, and upward ions are in the middle panel. In the bottom panel we display the PWI AC electric field data on a semilog plot with intense AKR extending down to frequencies near the local gyrofrequency, f_g (indicated by the black dotted line), in the time interval $0028 < t < 0030$. The somewhat "noisy" nature of the data is primarily a result of the compression of the data on the logarithmic frequency scale. The AKR extends to frequencies less than f_g which is to be expected when relativistic electrons are the dominant component. This follows directly from the relativistic gyroresonance condition for propagation at wave normal angles near 90° [cf. *Wu*, 1985]. Even though the auroral electrons of this pass are generally less than 10 keV, the relativistic correction is necessary in the theory of the cyclotron maser instability. The boundary plasma sheet (BPS) electrons are most energetic near 0028 UT, and the electron average energy decreases after 0029 UT. The intense electron flux in the energy range $4 \text{ eV} < E < 20 \text{ eV}$ is due to spacecraft photoelectrons. The upper energy extent of the upward flowing ions observed at the same time reached a maximum in the interval $0029 < t < 0030$ UT. Thus the potential below the spacecraft peaks at this time.

We have replotted the electron and PWI data at higher resolution in Plate 2. In this plot the electron data are shown at all pitch angles in the top panel and the AC magnetometer data from PWI are plotted in the bottom panel on a linear scale over a reduced frequency range. On this plot the proximity of the satellite to the AKR source region is more clearly noted. The usual criterion for determining if the satellite is near the AKR source center is that intense AKR is observed near the local gyrofrequency. We also indicate on this plot a region of temperature anisotropy ($T_\perp / T_\parallel > 1$) which corresponds to times

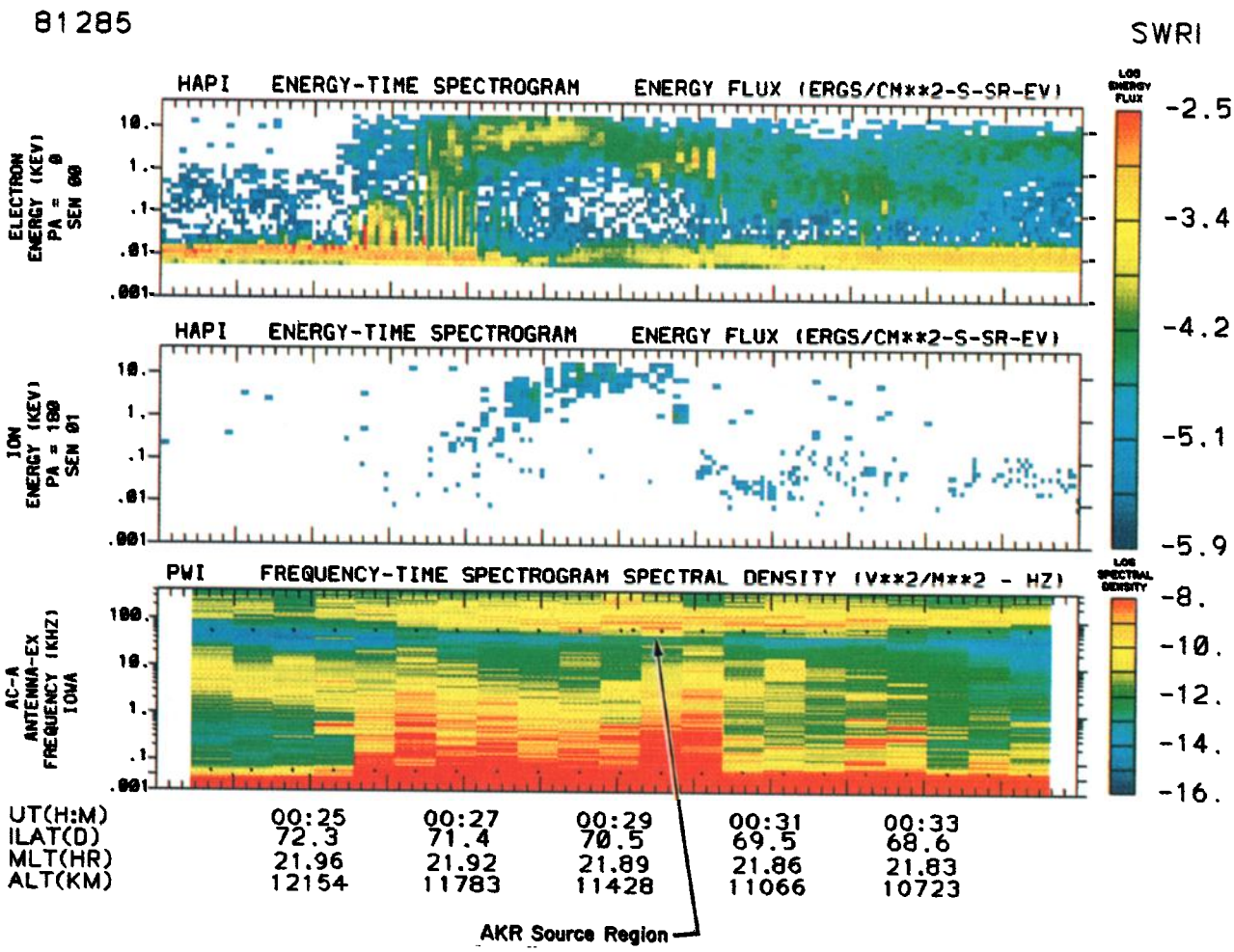

Plate 1. Energy versus time spectrogram with energy flux color coded for precipitating (top) electrons and (middle) upgoing ions. (Bottom) frequency versus time spectrogram with the electric field intensity color coded. The black dots indicate the local gyrofrequency for electrons (highest frequency) and ions.

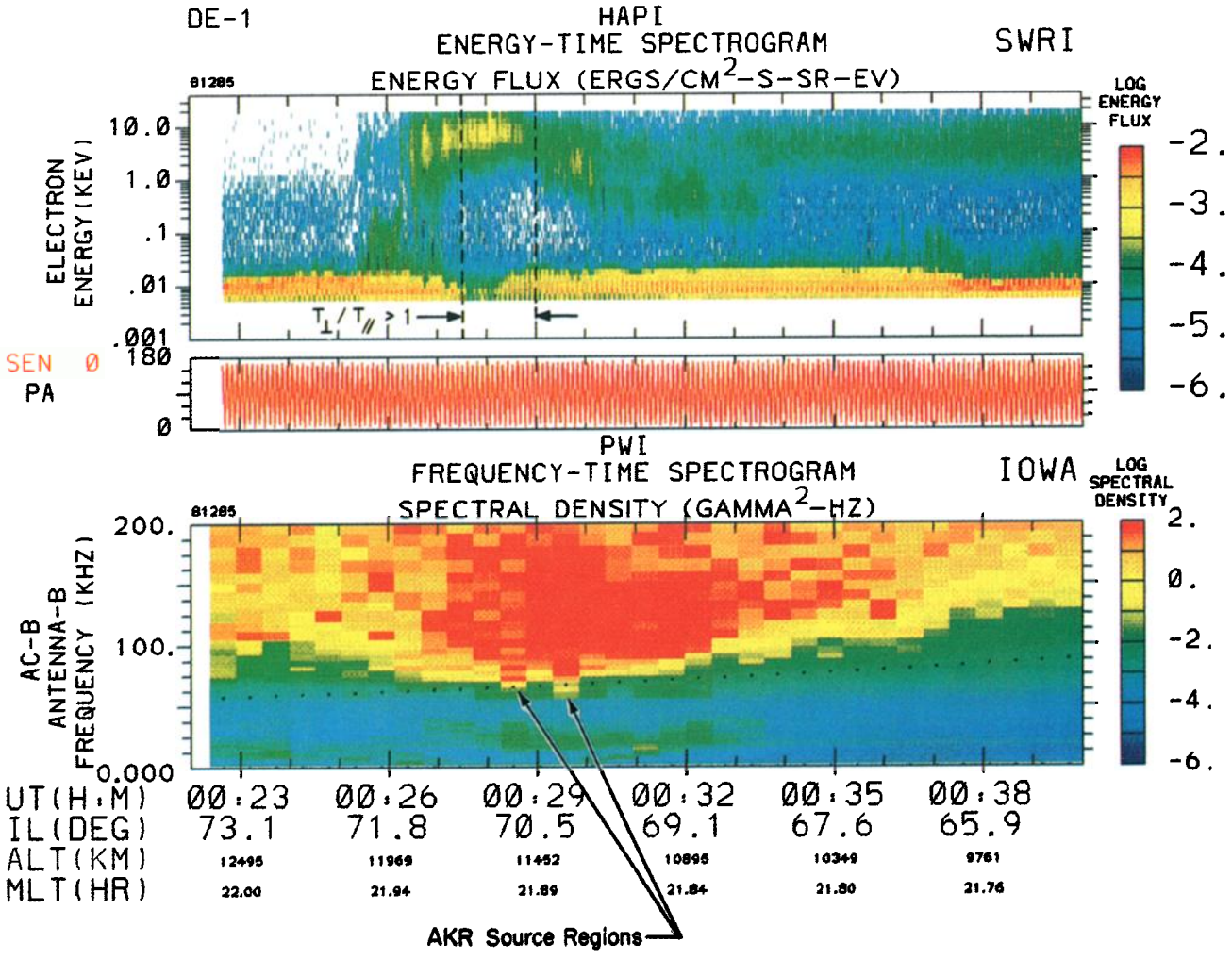

Plate 2. A higher-resolution spectrogram of the same pass as Plate 1. The electrons are displayed at all pitch angles in the top panel, and the magnetic field intensity is color coded in the bottom panel with the frequency plotted on a linear scale.

between about 0027:30 and 0029 as identified from the electron distribution discussed later. This region is adjacent to and extends into the AKR source region.

In Figure 1 we have plotted some of the calculated plasma parameters for an interval of this pass, including the times near the AKR source region. These parameters are evaluated from moments of the electron distribution function. To avoid inclusion of the spacecraft photoelectrons, the minimum energy of the integration is 23 eV. We see in Figure 1 that when the satellite is closest to the AKR source region, 0028 < t < 0030, a shallow density cavity (note the "notch" in the number flux) was encountered and the average electron energy was decreasing. Only a small decrease in density is observed because most of the cavity would exist in the thermal electrons which are not included in the density calculation shown. In Figure 2 we plot the temperature of the electrons versus invariant latitude. The temperature was calculated assuming a linear least squares fit to a Maxwellian. Each individual energy sweep was fitted for energies greater than the maximum energy of the spacecraft photoelectrons. There is a distinct peak just poleward of the AKR source center, in the region where $T_\perp/T_\parallel > 1$.

In Plate 3 we show the electron and ion data in the region nearest the AKR source center in higher resolution. Wide loss cones (that become semifilled for t > 0028:30) are observed throughout this time period, and the electric potential beneath the satellite reaches its peak in the range 0028:20 < t < 0029, as indicated by the upward ion beams. These beams have maximum energies equal to ~ 13 keV which was the programmed high-energy limit of the instrument at the time of the observations.

We now examine these data with the aid of phase space contour plots of the $\log_{10}$ of the distribution function in units of s^3/km^6. As noted in Plate 2, a region adjacent to and overlapping the AKR source region contained distributions with $T_\perp/T_\parallel > 1$. We show two examples of such distributions in Figure 3. The minimum energy is chosen in this and all other contours to avoid the spacecraft photoelectrons. In both of these figures the electron distributions show enhancements in the perpendicular direction continuously from the lowest energies to E > 2 keV well above photoelectron energies. It is possible that such distributions are the result of heating by wave-particle interactions. In this case the most likely waves are the emissions of AKR. We have estimated that for Figure 3*b*, $T_\perp/T_\parallel \sim 10$. We have carefully examined

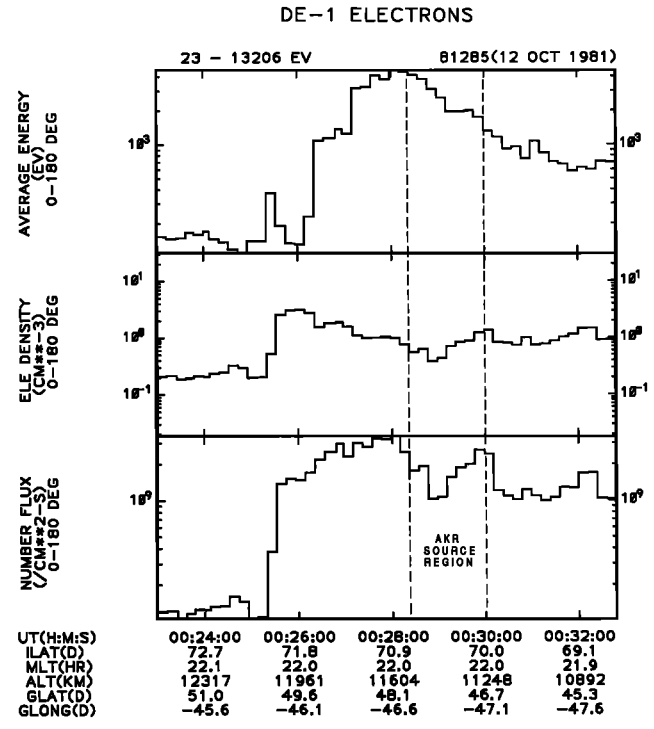

Fig. 1. Average energy, electron density, and number flux versus time for the pass of October 12, 1981. The times when the satellite was closest to the auroral kilometric radiation (AKR) source center are indicated by dashed lines.

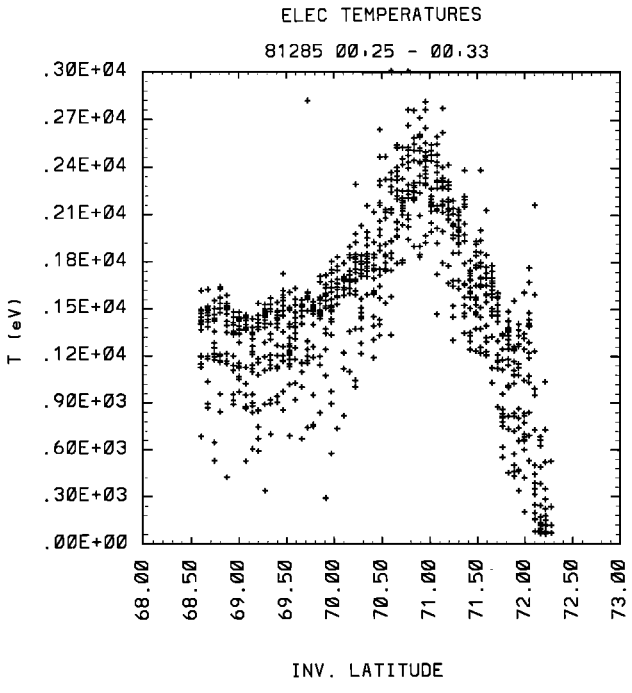

Fig. 2. Temperature versus invariant latitude for the pass of October 12, 1981.

high-resolution line plots (not shown) of the distribution function versus energy for each energy sweep during the times shown in the contour plots. It is clear that the enhancements shown in the distribution function at large pitch angle are statistically meaningful and that the most heating or diffusion occurs for the electron population with energies above several hundred electron volts. Electrons for energies less than a few hundred electron volts appear to be a separate and colder population. In other words, it appears that the magnetospheric electrons with energies greater than several hundred electron volts are being heated and/or diffused at large pitch angles. Also seen in both distributions of Figure 3 are field-aligned beams. The fact that these are distinct, statistically meaningful beams (and not holes, for instance) is demonstrated clearly by color contour plots, which are not shown. This is an example of a beam with temperature anisotropy of the kind *Newman et al.* [1988], *Wong and Goldstein* [1990] and *Winglee et al.* [1992] have shown is unstable to bursty radio emission via a modified kinetic Weibel or temperature anisotropic beam instability (TABI). We suggest this distribution may also be responsible for the broadbanded electromagnetic bursts recently reported by *Sonwalkar et al.* [1990].

The AKR source center is seen to consist of two separated regions of intense emission. Regions 1 and 3 are separated by region 2, from about 0028:50 to about 0029:20 where the AKR intensity slightly decreases. We do not know if this decrease is a temporal or spatial effect. Within region 1 the distribution of electrons includes semifilled loss cones and trapped particles, and temperature anisotropies as shown in Figures 4*a*-4*d*. In region 2 the distributions include semifilled loss cones and an electron conic (5*c*), as shown in Figures 5*a*-5*d*. We hypothesize the electron conic may be the result of wave-particle heating resulting from the AKR emission. Wave-particle interactions resulting in electron conics has been suggested by *Wong et al.* [1988], *Temerin and Cravens* [1990], and *Menietti et al.* [1992]. Within region 3 the loss cone features are not as prevalent, but more beamlike distributions are observed, as displayed in Figures 6*a*-6*d*. Also observed in both regions 2 and 3 are "banana" distributions (so named because of the shape of the beam), as shown in Figures 5*b*, 5*d*, 6*c*, and Figure 7. The features are statistically meaningful beams as observed on color contours and detailed plots of distribution function versus energy (not shown). Such distributions are the result of beams that have been spread in pitch angle due to the conservation of the first adiabatic invariant [cf. *Winglee and Pritchett*, 1986]. In Figure 7 we show in greater resolution a distribution that appears to be a combination of a banana distribution and a "trapped" population. It takes 6 s to sample the data required for the contour plot. The data sampling began at the data point indicated and proceeded in the counterclockwise direction. Thus the "banana" was sampled in the early part of the satellite spin and the "trapped" distribution was sampled near the end of the spin. It is possible that the banana distribution may have been unstable to cyclotron maser emission which heated the electron population, causing diffusion that produced the "trapped" distribution observed later in the same satellite spin.

Winglee and Pritchett [1986] have examined with the aid of numerical simulations how such distributions lead to the generation of electrostatic as well as AKR emissions. In their Figure 1 they show schematically how a field-aligned beam of electrons, as produced in an acceleration region, is spread in pitch angle due to the conservation of the first adiabatic invariant. In

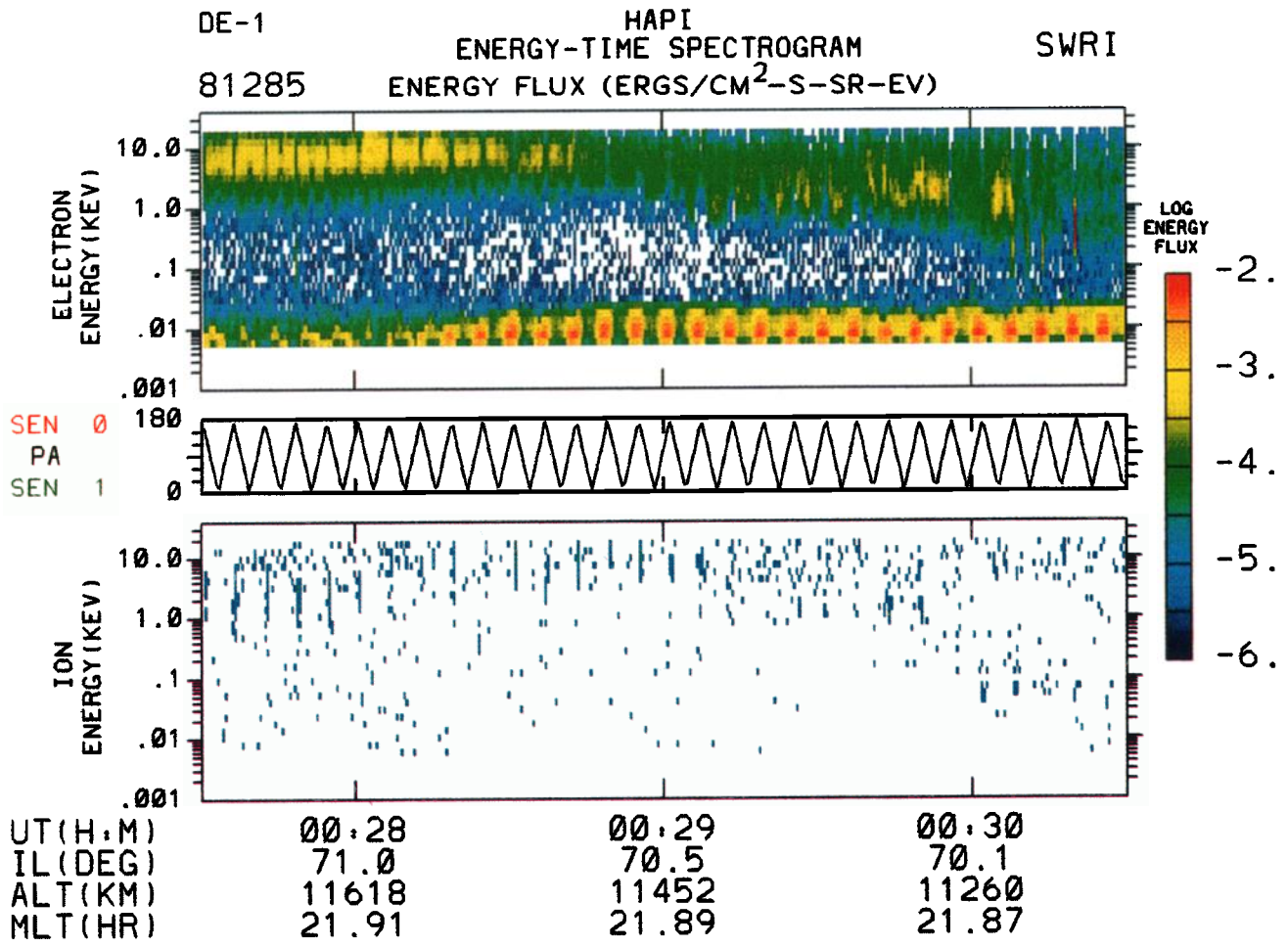

Plate 3. (Top) high-resolution spectrogram of electron and (bottom) ion energy flux. The upward ion beams indicate a field-aligned potential beneath the satellite. For times greater than about 0029 UT the energy flux and average energy of the electrons decreased.

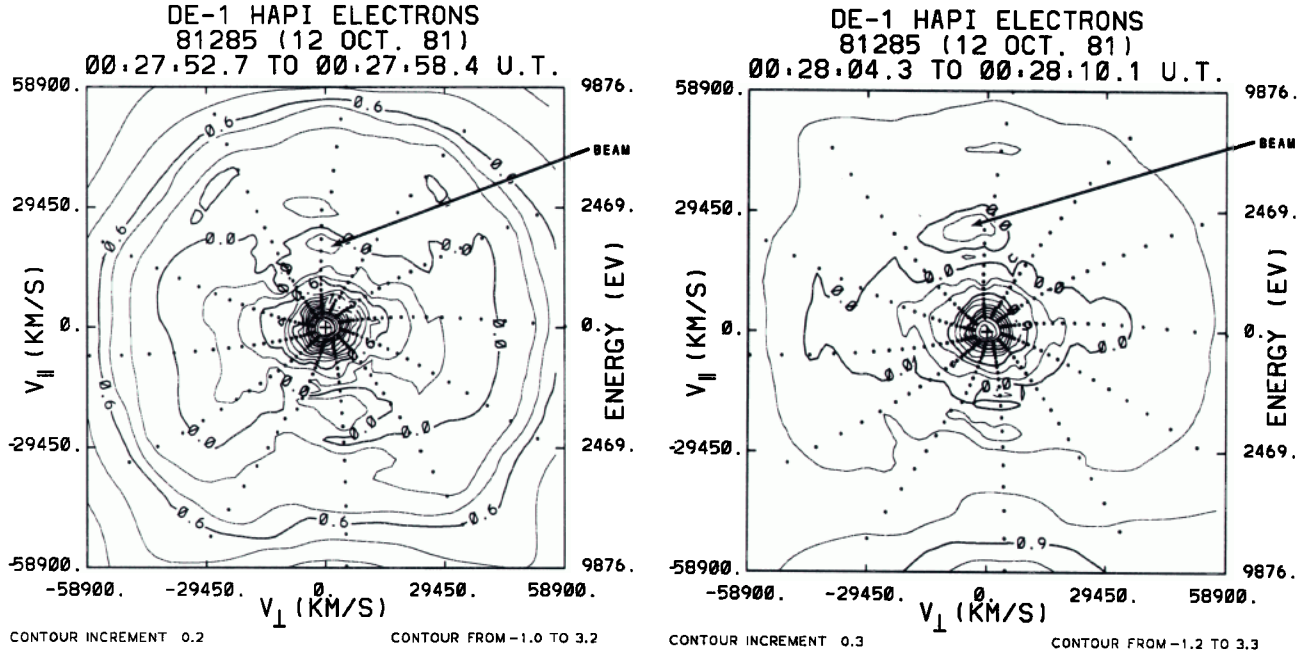

Fig. 3. Contours of the distribution function in phase space obtained adjacent to and poleward of the AKR source region. Both of these examples show strong anisotropies with $T_\perp > T_\parallel$.

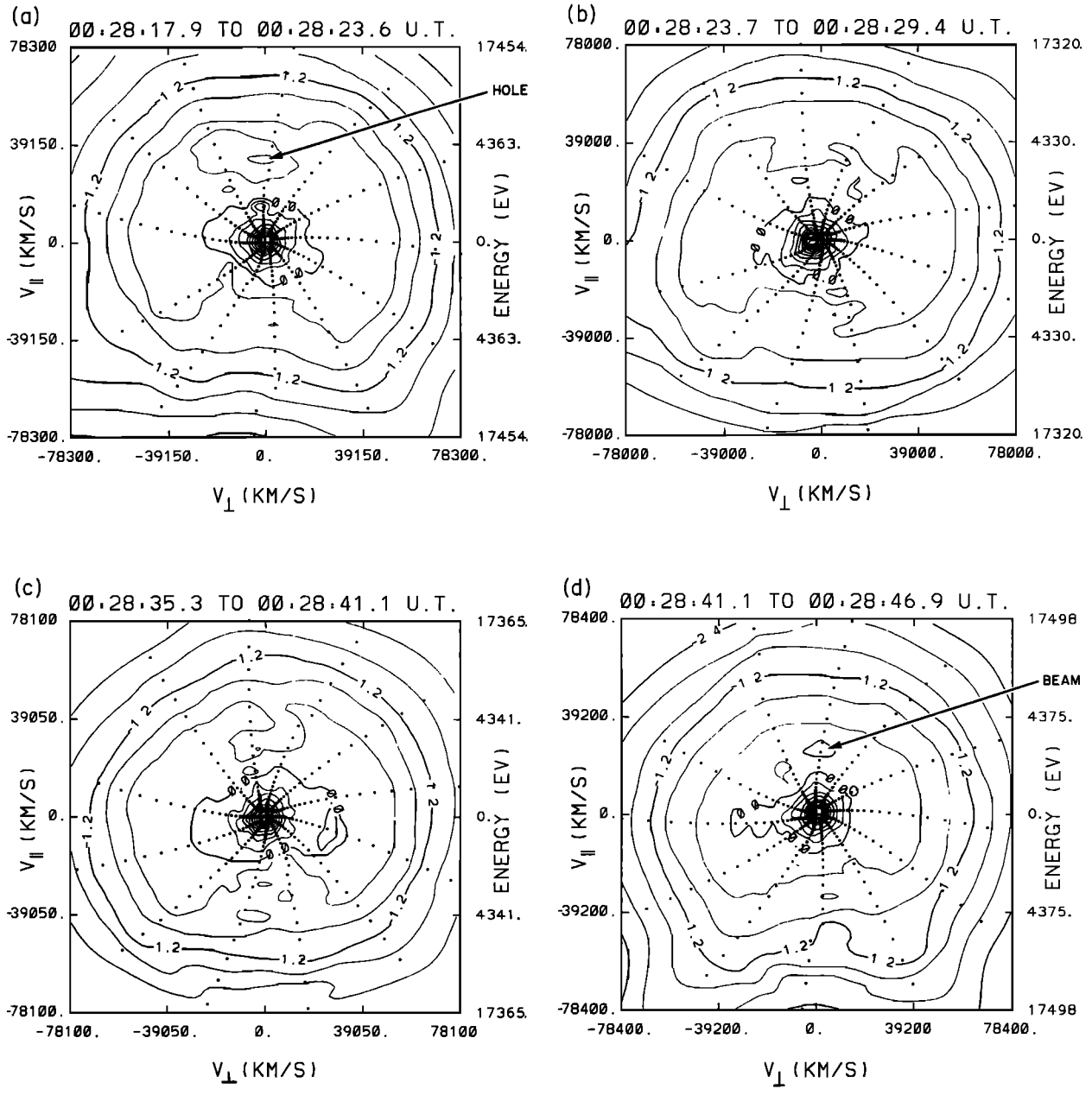

Fig. 4. A series of contours of the distribution function obtained when the satellite was in region 1 (0028:20 < t < 0028:50). Note the presence of (4*a*-4*d*) semifilled loss cones, (4*a*-4*d*) temperature anisotropies with $T_\perp > T_\parallel$, and (4*d*) an electron conic.

their Figure 7, Winglee and Pritchett schematically show how such banana distributions contain both $\partial f/\partial v_\parallel > 0$ and $\partial f/\partial v_\perp > 0$ and are thus unstable to both the bump-in-tail and the cyclotron maser instability. In Figure 8 we reproduce contours of the distribution function as calculated from two-dimensional simulations [cf. *Winglee and Pritchett*, 1986, Figure 14]. Note that diffusion of the distribution function resulting from the bump-in-tail instability as well as the cyclotron maser instability drive the distribution to a more isotropic state. The similarity of some of the distributions shown in Figure 8 to those of Figures 5 and 6 is apparent. We conclude from this comparison that it is probable that the observed distributions are the result of wave-particle interactions.

Pass of October 4, 1981 (Day 277)

Plate 4 displays the data for October 4, 1981, in the same format as Plate 1. In Plate 5 we show the higher-resolution electron data together with the AC electric field data plotted on a linear scale. Field-aligned potentials indicated by enhanced precipitating electron flux and upward flowing ions are seen periodically in the interval from about 0727 to 0735:30. Typical potential differences above and below the satellite are each about 5 kV. The satellite is nearest to the AKR source region during the time interval 0735:15 < t < 0739:30. In this time interval, intense AKR emission extends to frequencies less than the local gyrofrequency. Adjacent to and within this region the electron

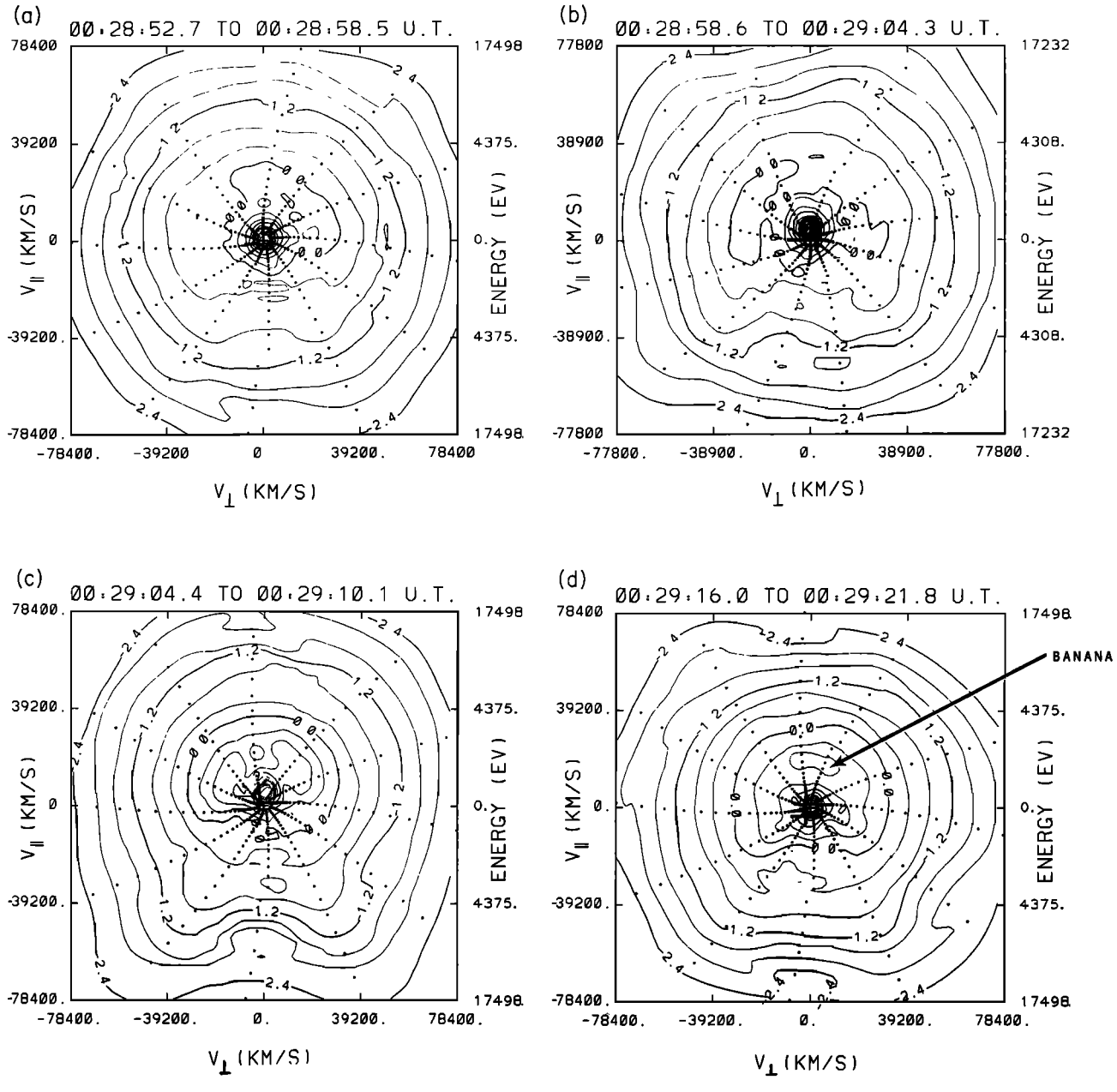

Fig. 5. A series of contours of the distribution function obtained when the satellite was in region 2 (0028:50 < t < 0029:20). The salient features are (*5a-5d*) semifilled loss cones and (*5d*) a banana distribution, but the temperature anisotropies are not as large as in region 1.

particle data contain loss cones, "banana distributions," and electron conics. In Figure 9 we show a series of contour plots within this region with these features indicated. It is possible that the "trapped particles" of Figure 9*a* may be a part of the banana distribution and therefore formed by conservation of the first adiabatic invariant. We again point out the similarity of these distributions to those simulated by *Winglee and Pritchett* [1986]. Figure 9*c* is an example of an electron conic observed at this time that may be due to local oblique heating of the electrons due to wave-particle interactions [cf. *Menietti et al.*, 1992]. Figure 10 contains two examples of distributions obtained closer to the AKR source region. These plots show semifilled loss cones and distributions with $T_\perp/T_\parallel > 1$ which we suggest are due to perpendicular heating of electrons due to the AKR. Examination of high-resolution plots of the distribution function versus energy indicate that the peaks in the distribution function are statistically meaningful and that electron heating or diffusion occurs for electrons with energies greater than several hundred electron volts.

Plasma parameters for this pass are plotted in Figure 11. Similar to Figure 1 we note that the AKR source region occurs in the region of decreasing average energy. The density cavity is not as discrete for this pass as in Figure 1, but density decreases occur corresponding to the number flux minima (notches). One

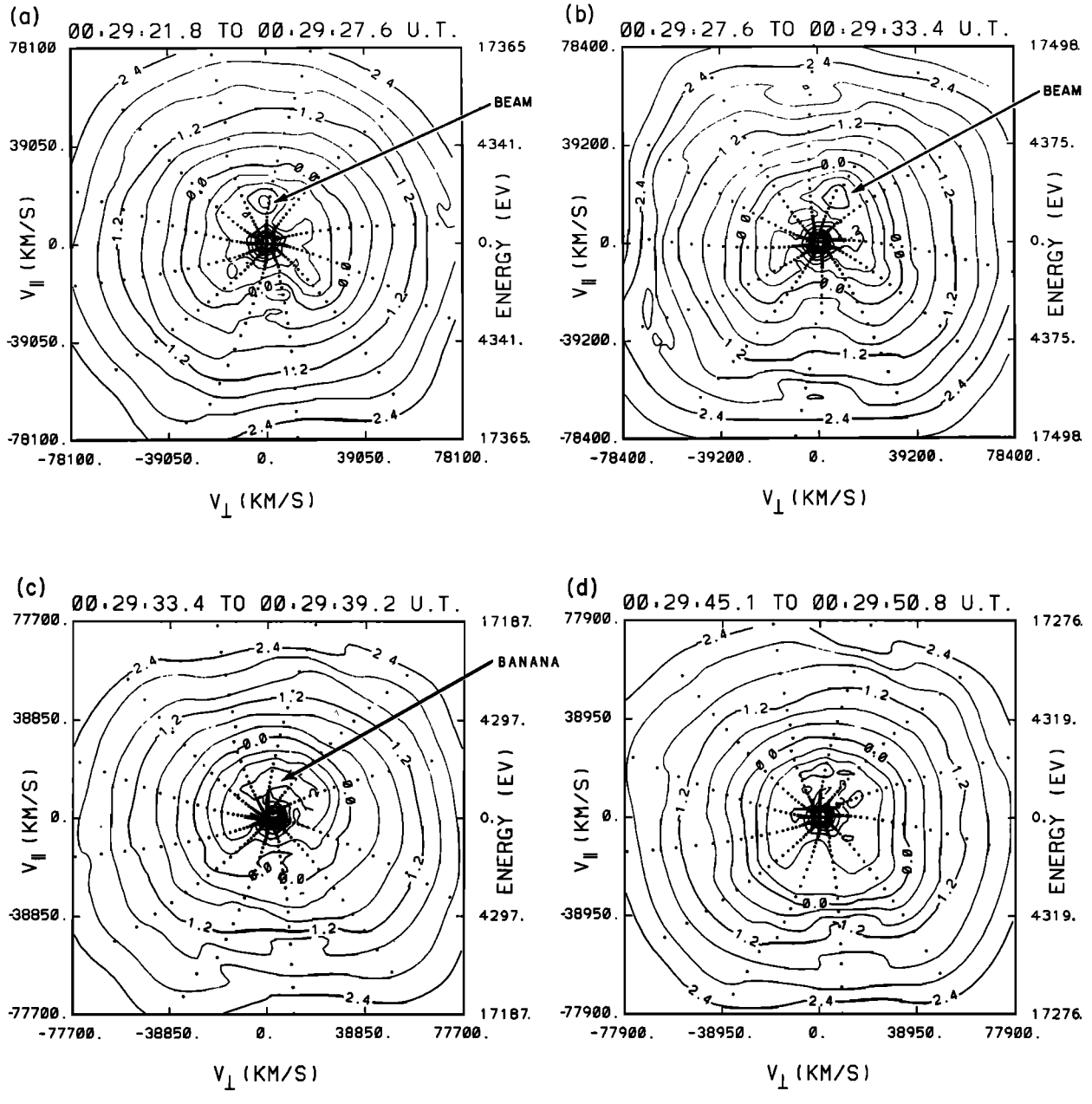

Fig. 6. Same as Figures 4 and 5, but now for region 3 (0029:20 < t < 0030). A banana distribution appears in 6*c*, and an electron conic is observed in 6*d*.

explanation for this is that the satellite could be passing next to, rather than through, the AKR source region. This is further indicated by the lack of significant field-aligned potential either above or below the satellite. It is also true, as explained earlier, that the largest density cavity would occur in the thermal electrons, which are not included in the integrations for the moments.

Pass of September 27, 1981 (Day 270)

The final example is the pass of September 27, 1981. Plates 6 and 7 display the electron and AC magnetometer data for this pass in the same formats as before. Field-aligned potentials both above and below the satellite which at some times reach about 10 kV are seen in the interval from about 1048 to 1053. In the time interval from about 1054:30 to about 1057:30, most of the potential difference is below the satellite (~ 7 kV), with about 2 kV above the satellite in the smaller time interval from about 1056 to 1058. The satellite is nearest the source of the AKR in the time interval 1055:30 < t < 1057:30, with perhaps the closest approach (judging from the lowest frequency of AKR) occurring in the interval 1055:30 < t < 1056. The plasma parameters plotted in Figure 12 indicate a shallow density cavity centered around 1053 UT but not when the satellite was closest to the AKR source center. For this pass the average energy of the electrons seems to be almost constant when the satellite is closest to the AKR region but lower than the energy of the BPS electrons encountered in the time interval 1048 to 1052. The AKR source

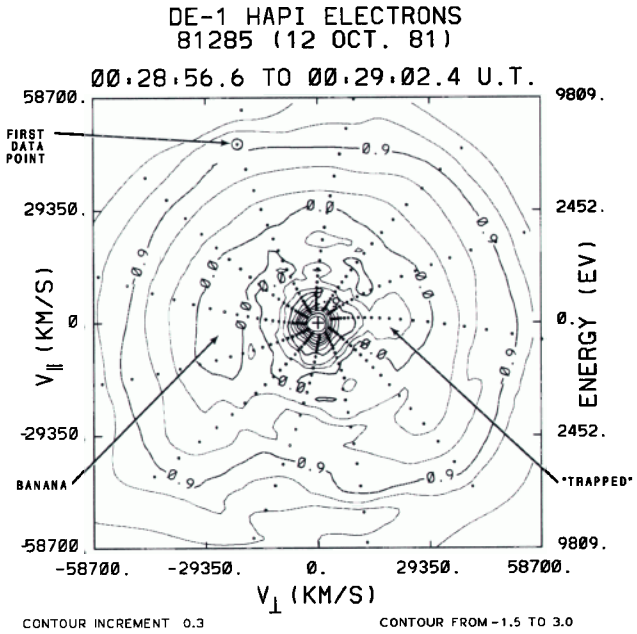

Fig. 7. A high-resolution plot of Figure 6*b*. The banana distribution has apparently been extended in pitch angle due to the conservation of the first adiabatic invariant. Perhaps local heating due to wave-particle interactions has produced the "trapped" distribution seen (see text).

region is thus coincident with a region of field-aligned potential most of which is beneath the satellite, as evidenced by the energetic upward ions seen in the middle panel of Plate 6.

Contours of the electron distribution function obtained during this time indicate that loss cones, trapped particles, and a large region where $T_{\perp}/T_{\parallel} > 1$ exist when the satellite was nearest the AKR source region. The region where $T_{\perp}/T_{\parallel} > 1$ is in the range $1055 < t < 1057{:}40$, as indicted in Plate 7. For this pass, most of the examples of $T_{\perp}/T_{\parallel} > 1$ occur equatorward rather than poleward of the source. In Figure 13 we show some exemplary contours during this time period, indicating the salient features. Distributions with $T_{\perp}/T_{\parallel} > 1$ are seen in Figures 13*a*, 13*c* and 13*d*, whereas trapped particles are seen in Figure 13*b*. The distinction is that in Figures 13*a*, 13*c*, and 13*d* the distribution function is enhanced perpendicular to **B** from lower energies, whereas in Figures 13*b* the distribution has an elliptical shape (no enhancement at the lowest energies along $v_{\perp}$). This latter case is the typical signature of trapped particles suggested by the work of *Knight* [1973], with trapped particles lying in an oval-shaped region along the $v_{\perp}$ axis. Examination of detailed distributions (not shown) indicate most of the electron heating and/or diffusion occurs for electron energies greater than several hundred electron volts. For this pass, due to the lack of significant potential difference above the satellite when it is nearest the AKR source region, there are no significant banana distributions.

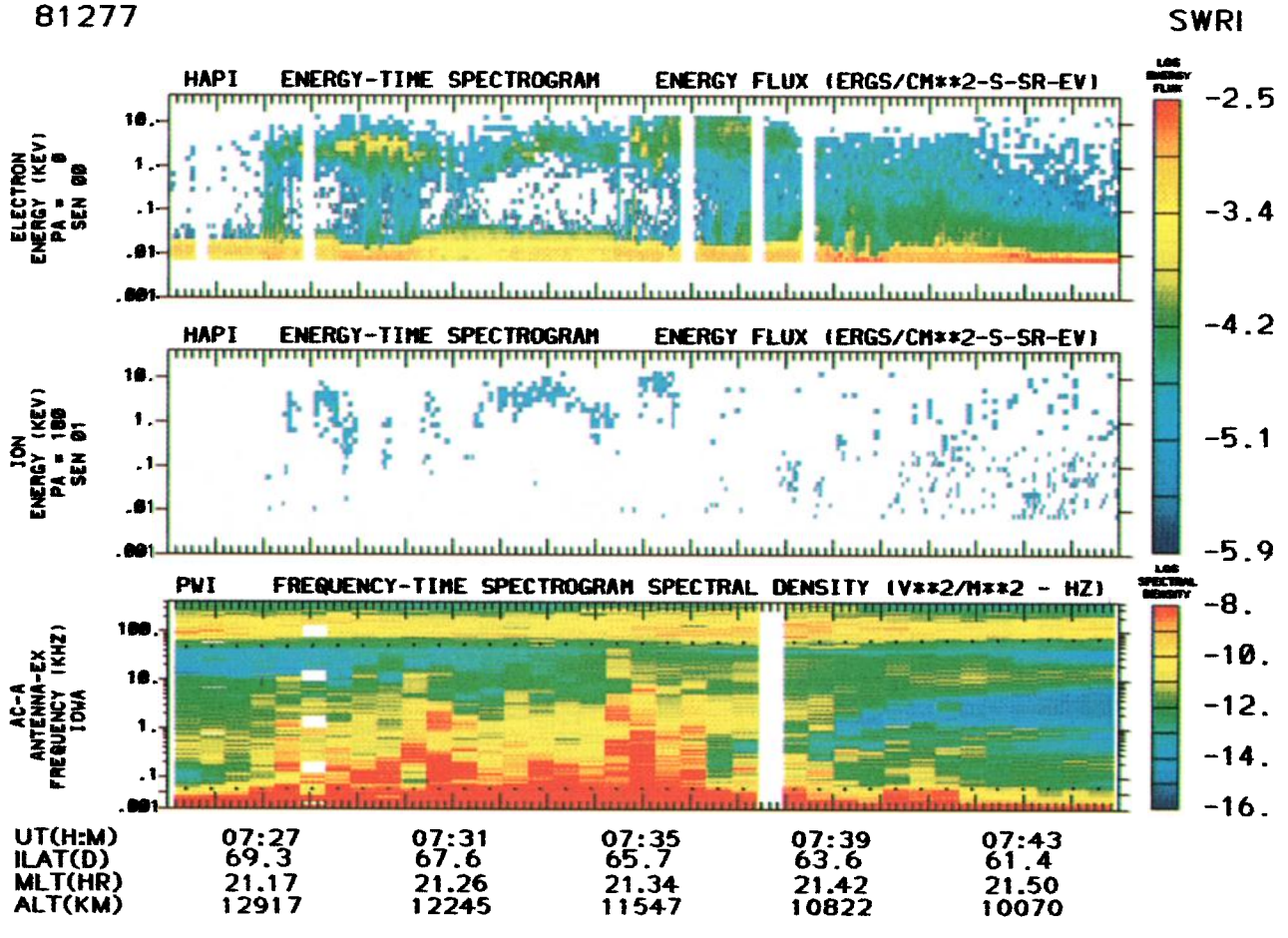

Plate 4. Particle and wave intensity spectrograms in the same format as Plate 1 but now for the pass of October 4, 1981.

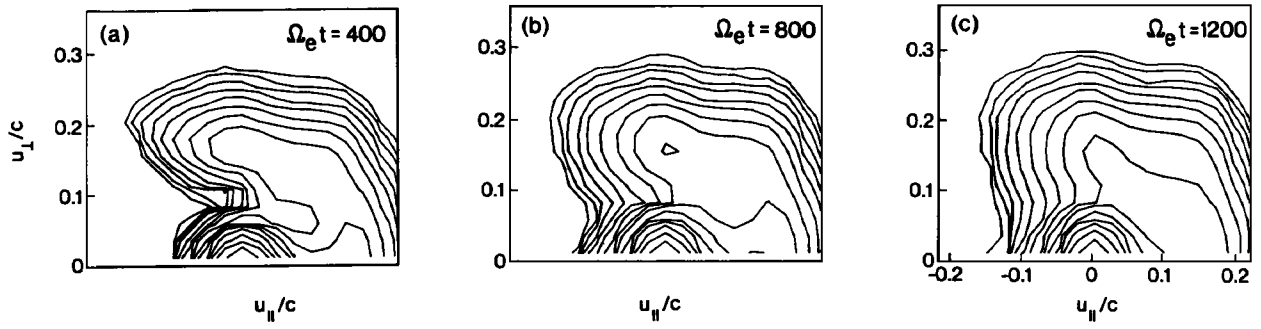

Fig. 8. A reproduction of Figure 14 of *Winglee and Pritchett* [1986]. This series of contours of the distribution function are the results of numerical simulation of an initial banana distribution. The isotropization is due to wave-particle interactions and diffusion of the electrons that have been heated both perpendicular and parallel to the magnetic field direction. These figures resemble many of the contours of Figures 4, 5, and 6.

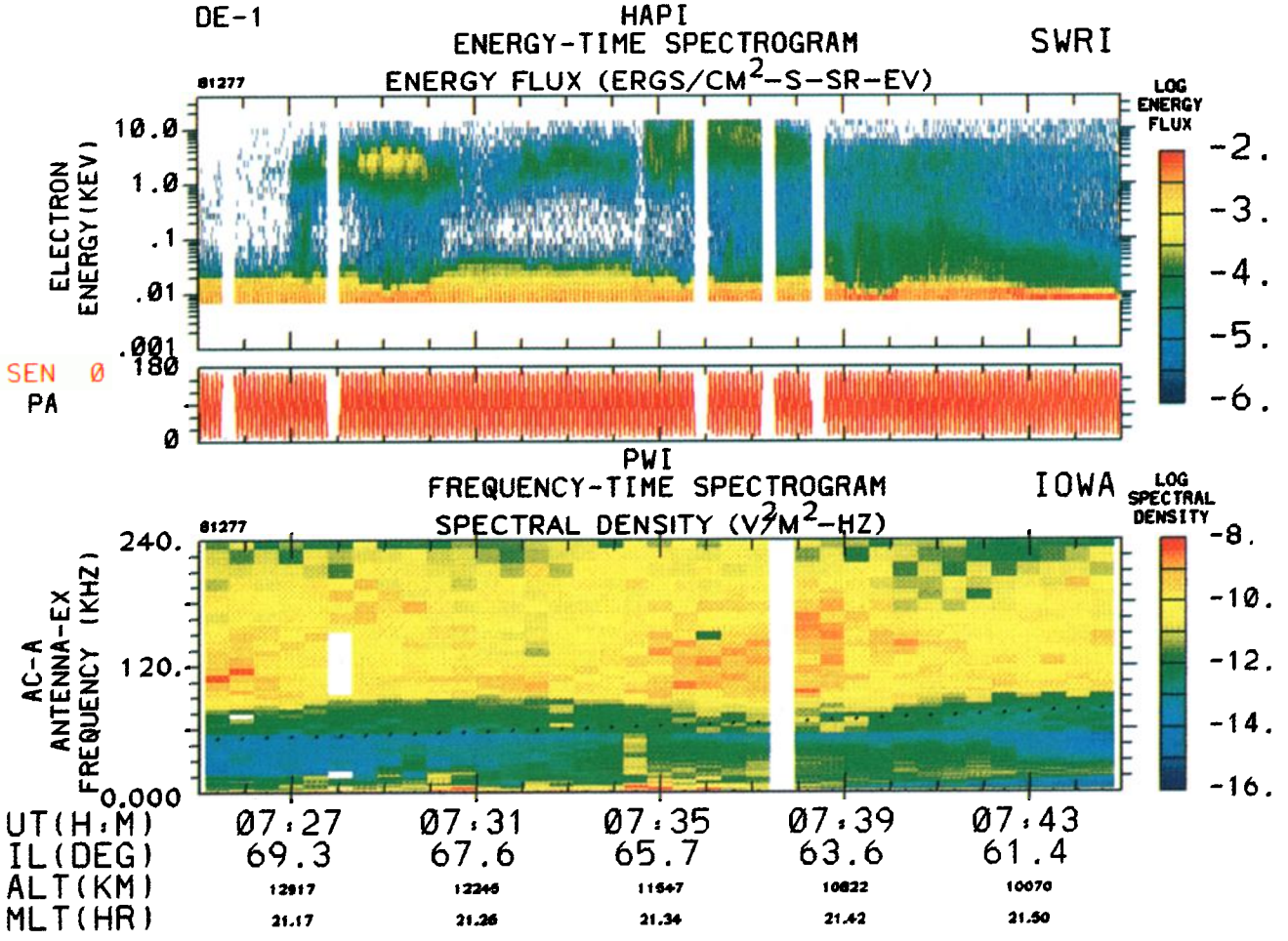

Plate 5. Higher-resolution spectrograms for the pass of October 4, 1981.

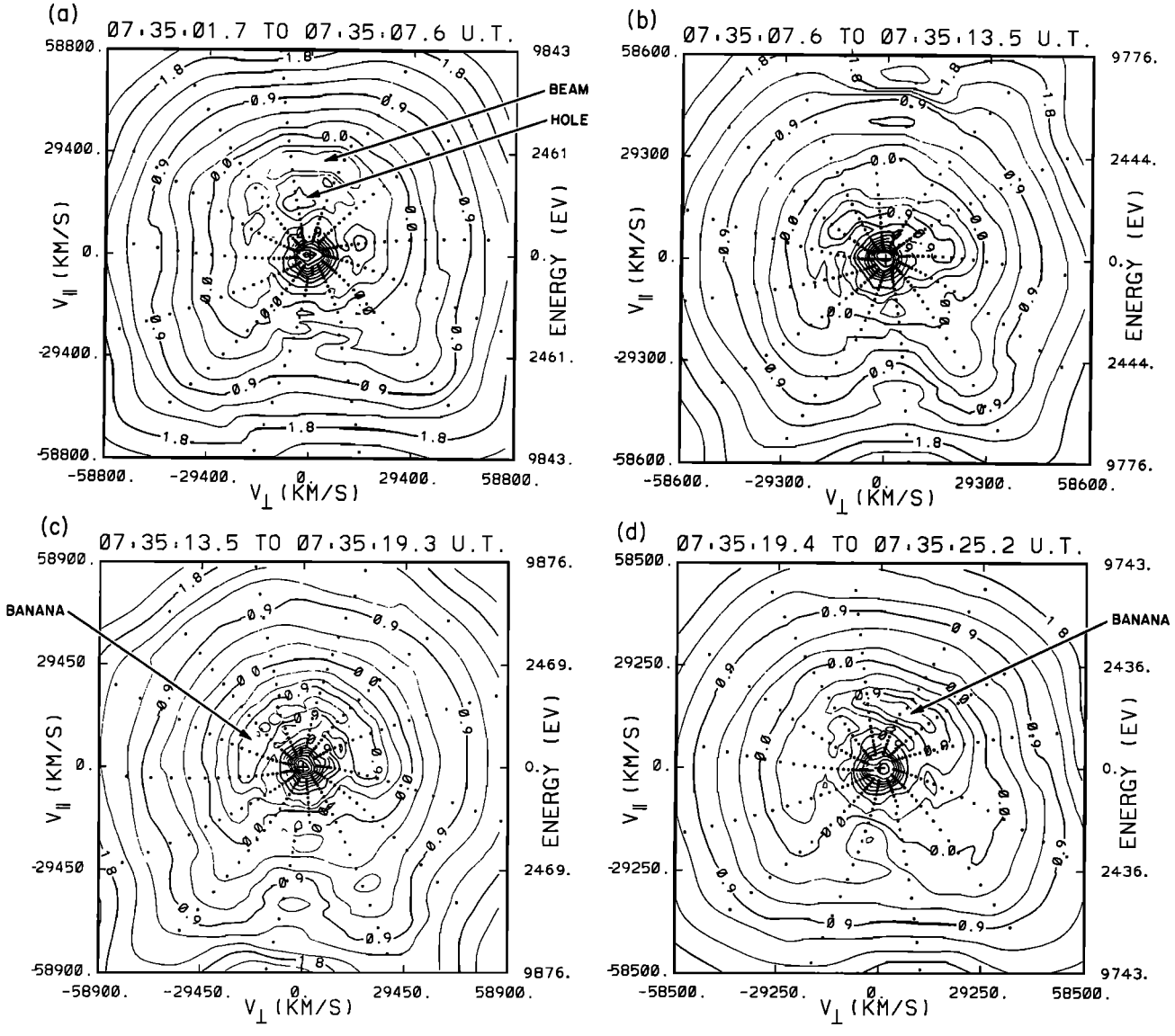

Fig. 9. Contours of the distribution function when the satellite was near the AKR source region for the pass of October 4, 1981. Note the presence of banana distributions, loss cones, and an electron conic (9*c*).

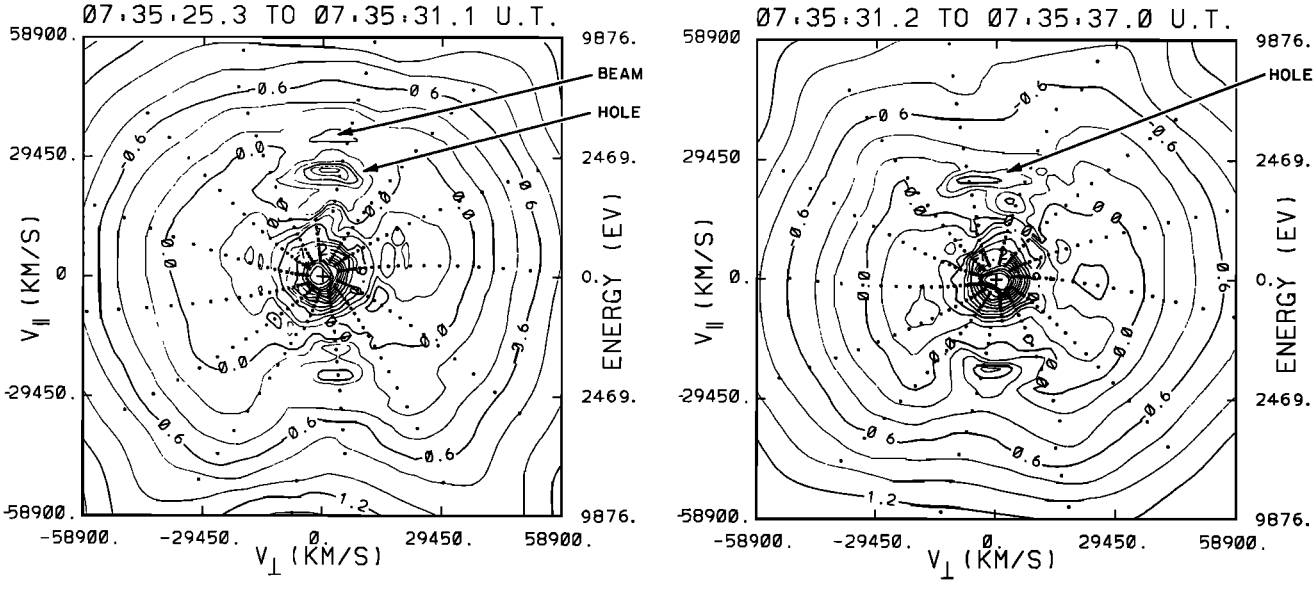

Fig. 10. Two examples of temperature anisotropies seen near the AKR source region for the pass of October 4, 1981.

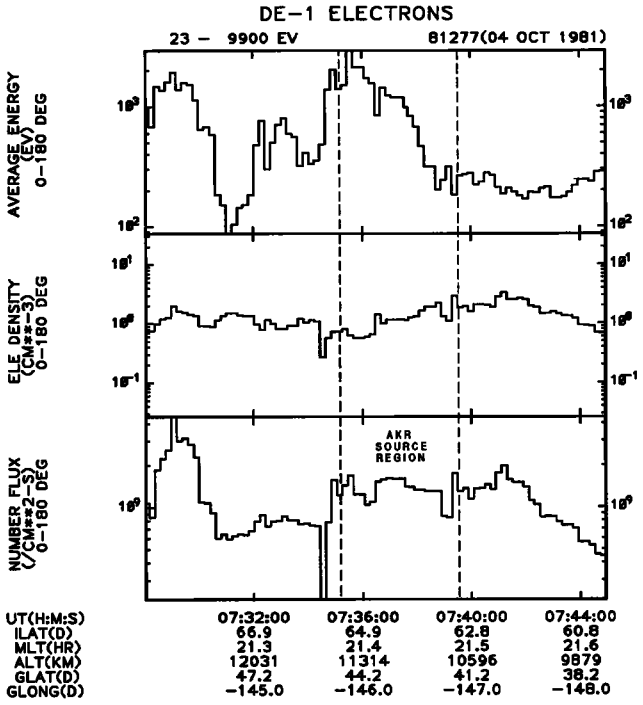

Fig. 11. Same as Figure 1 but for the pass of October 4, 1981.

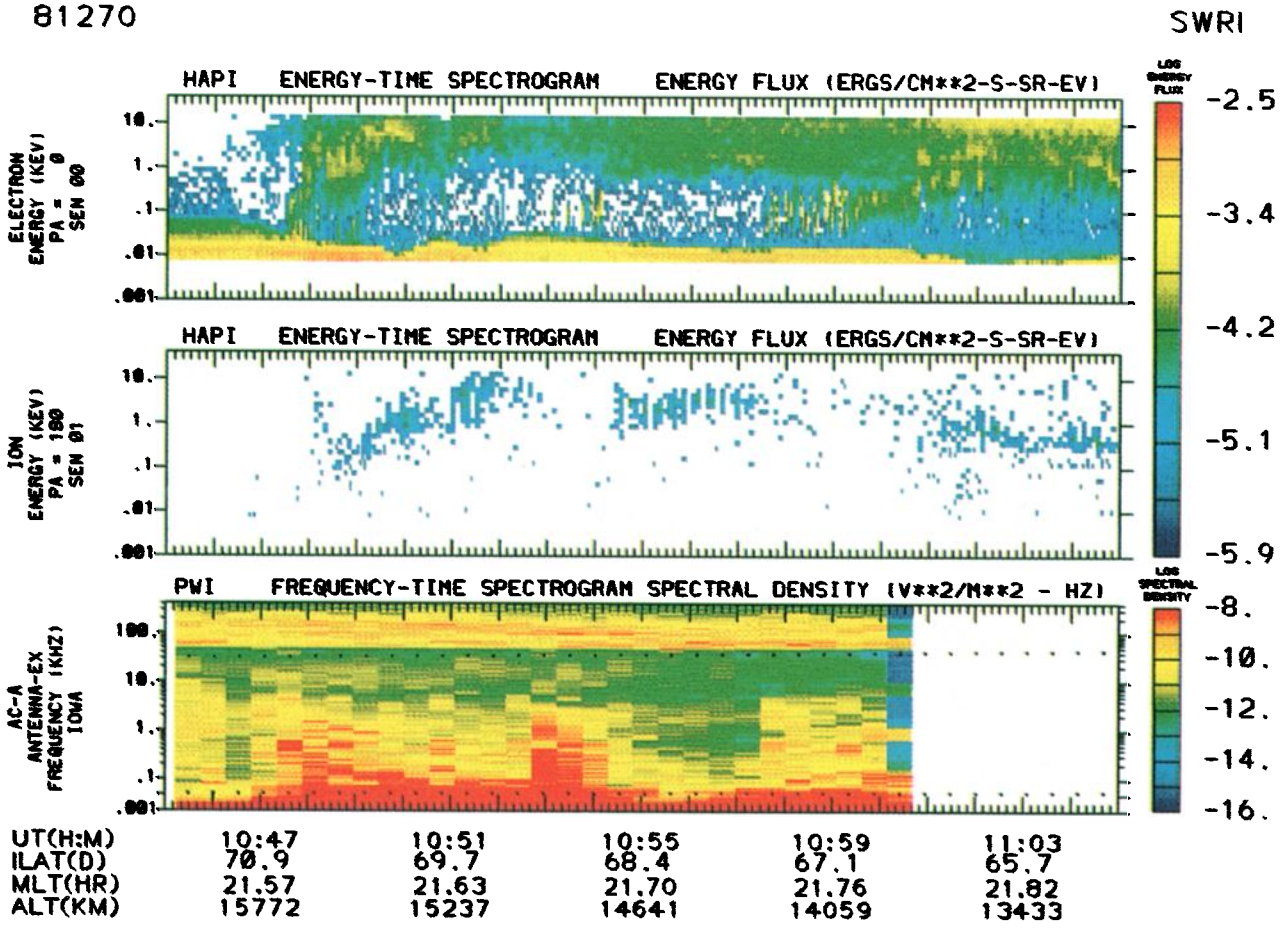

Plate 6. Particle and wave intensity spectrograms for the pass of September 27, 1981.

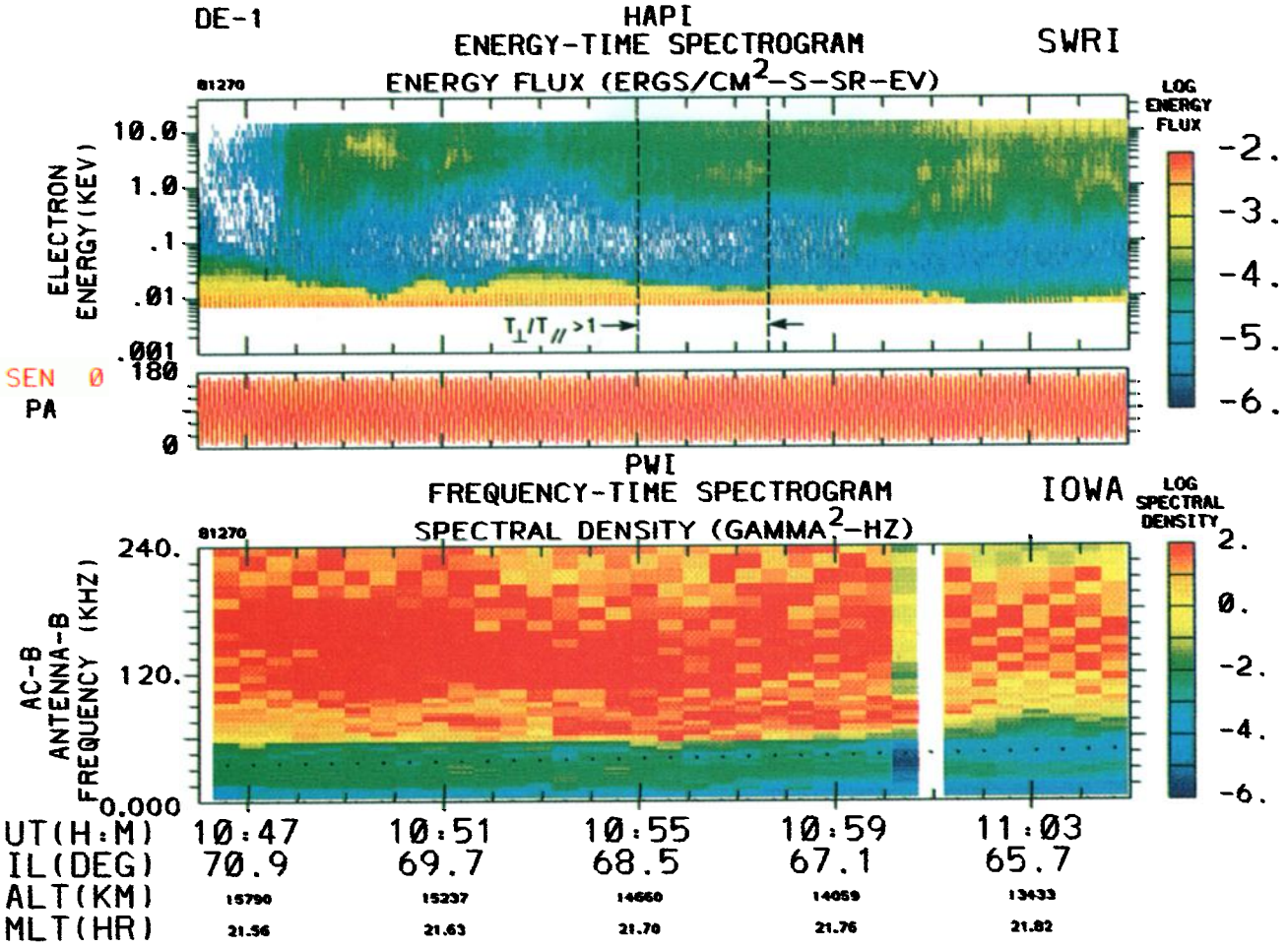

Plate 7. Higher-resolution spectrograms for the pass of September 27, 1981.

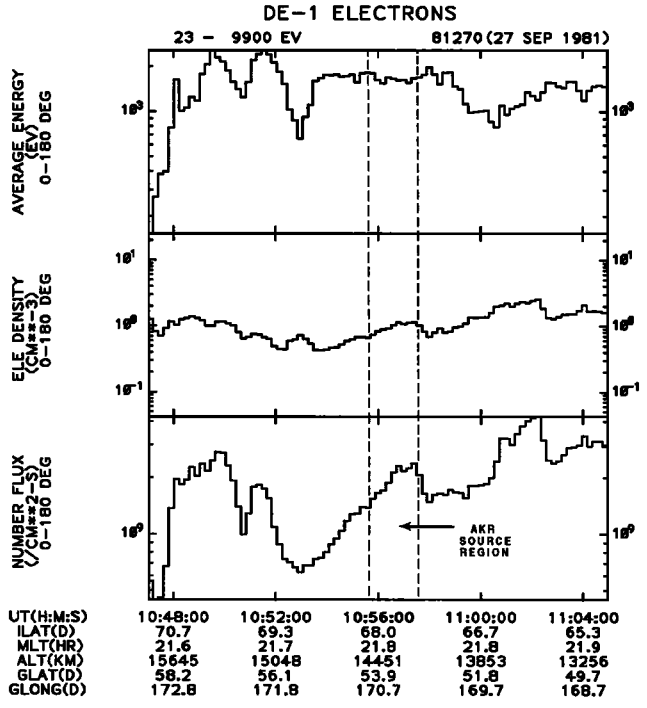

Fig. 12. Plasma moments for the pass of September 27, 1981.

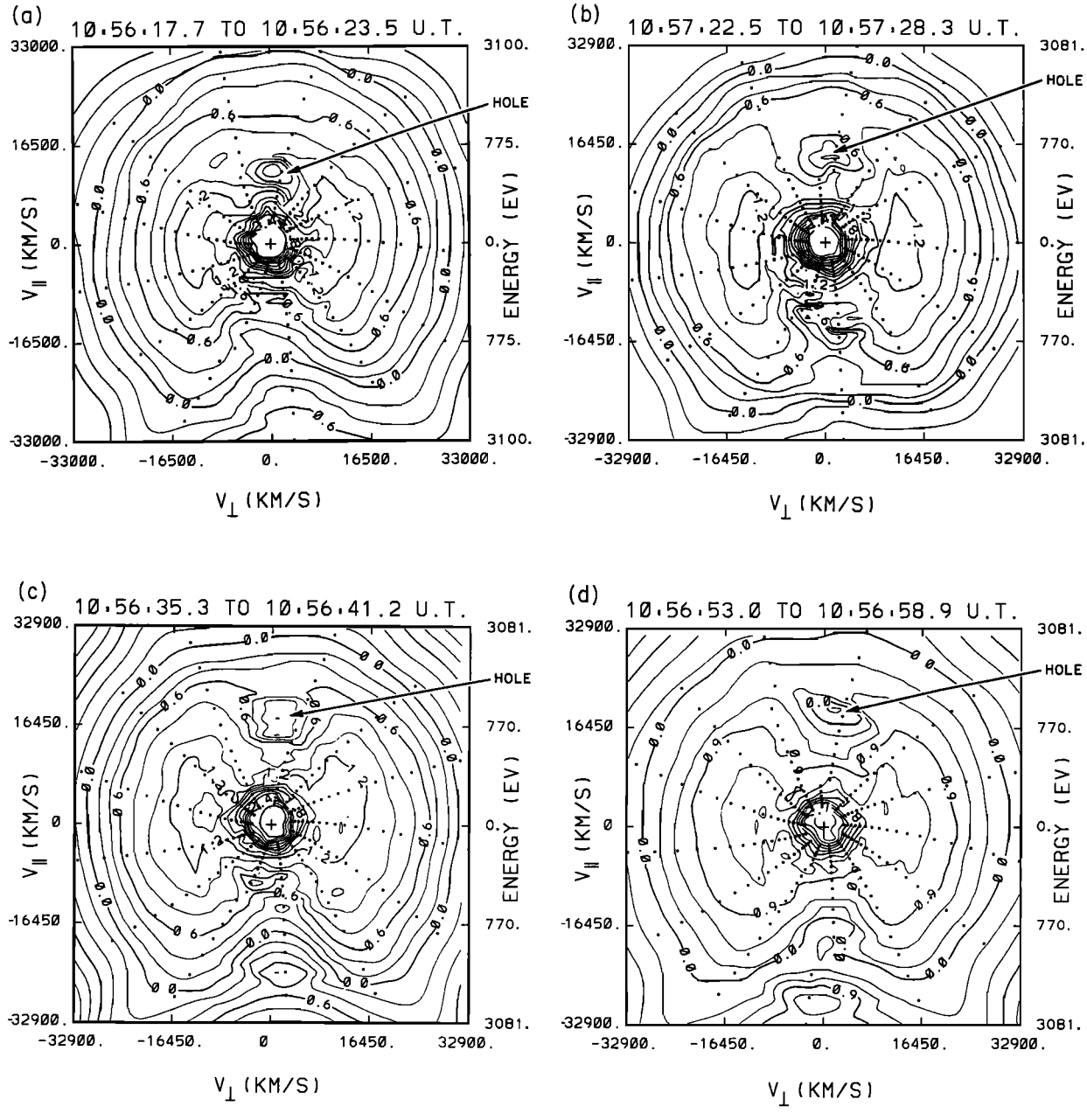

Fig. 13. A series of exemplary contours of the distribution function for the pass of September 27, 1981. Note the presence of loss cones and large temperature anisotropies with $T_\perp > T_\parallel$.

SUMMARY AND CONCLUSIONS

We have presented examples of electron distributions as observed by the high-altitude plasma instrument as the DE 1 satellite passed near AKR source regions. For each example, loss cones (some semifilled) were observed when the satellite was closest to the AKR source region, and temperature anisotropies in the distribution and electron conics were observed sometimes within and sometimes adjacent to the source region. These data are consistent with the hypothesis that perpendicular heating due to wave-particle interactions occurs near the AKR source region, thus modifying the "source" distribution.

The observations indicate that it is difficult to determine whether trapped particles are the source or the result of AKR emission, as has been suggested by *Louarn et al.* [1990]. Our results are in agreement with *Ungstrup et al.* [1990] who find the electron distributions are considerably modified by the waves near the AKR source region. The results of *Winglee and Pritchett* [1986] indicate that "banana" distributions commonly observed in acceleration regions of the nightside auroral region are unstable to AKR emission which in turn heats the electron distribution and results in an isotropization of the electron population, which could lead to distributions that resemble trapped distributions (compare Figure 7). To resolve the outstanding problems, it will be necessary to obtain multiple and simultaneous measurements both outside and inside the AKR source region by both particle and wave instruments. More detailed modeling and simulations which incorporate the structure of the source region, as described above, are also needed to help identify sources and sinks for the observed waves and the details of the wave-particle interactions.

Acknowledgements. We gratefully acknowledge many useful discussions of these observations with Kit Wong. We wish to thank Glenda Perez, Kathy Kurth, and Michelle Govostes for clerical assistance and Tony Sawka for drafting some of the figures. This research was supported at SwRI by NASA grants NAS5-28711 (JDM and JLB) and NAG5-1552 (JDM); and at the University of Iowa by NAG5-2102 and NAGW-3143.

The Editor thanks L. R. Lyons and M. A. Temerin for their assistance in evaluating this paper.

REFERENCES

Benson, R. F., and W. Calvert, ISIS I observations at the source of auroral kilometric radiation, *Geophys. Res. Lett.*, *6*, 479, 1979.

Burch, J. L., J. D. Winningham, V. A. Blevins, N. Eaker, W. C. Gibson, and R. A. Hoffman, High-altitude plasma instrument for Dynamics Explorer-A, *Space Sci. Instrum.*, *5*, 455, 1981.

Dusenbury, P. B., and L. R. Lyons, General concepts on the generation of auroral kilometric radiation, *J. Geophys. Res.*, *87*, 7467, 1982.

Green, J. L., D. A. Gurnett, and R. A. Hoffman, A correlation between auroral kilometric radiation and inverted V electron precipitation, *J. Geophys. Res.*, *84*, 5216, 1979.

Gurnett, D. A., The Earth as a radio source: Terrestrial kilometric radiation, *J. Geophys. Res.*, *79*, 4227, 1974.

Hilgers, A., The auroral radiating plasma cavities, *Geophys. Res. Lett.*, *19*, 237, 1992.

Knight, S., Parallel electric fields, *Planet. Space Sci.*, *21*, 741, 1973.

LeQueau, D., R. Pellat, and A. Roux, *Phys. Fluids*, *27*, 247, 1984.

Lin, C. S., J. L. Burch, C. Gurgiolo, and C. S. Wu, DE 1 observations of hole electron distribution functions and the cyclotron maser resonance, *Ann. Geophys.*, *4*, 33, 1986.

Louarn, P., A. Roux, H. de Feraudy, D. LeQueau, M. Andre, and L. Matson, Trapped electrons as a free energy source for the auroral kilometric radiation, *J. Geophys. Res.*, *95*, 5983, 1990.

Menietti, J. D., C. S. Lin, H. K. Wong, A. Bahnsen, and D. A. Gurnett, Association of electron conical distributions with upper hybrid waves, *J. Geophys. Res.*, *97*, 1353, 1992.

Newman, D., R. M. Winglee, and M. V. Goldman, Theory and simulation of electromagnetic beam modes and whistlers, *Phys. Fluids*, *31*, 1515, 1988.

Omidi, N., and D. A. Gurnett, Growth rate calculations of auroral kilometric radiation using the relativistic resonance condition, *J. Geophys. Res.*, *87*, 2377, 1982.

Omidi, N. A., C. S. Wu, and D. A. Gurnett, Generation of auroral kilometric and Z-mode radiation by the cyclotron maser mechanism, *J. Geophys. Res.*, *89*, 833, 1984.

Sharp, R. D., R. G. Johnson, and E. G. Shelley, Energetic particle measurements from within ionospheric structures responsible for auroral acceleration processes, *J. Geophys. Res.*, *84*, 480, 1979.

Shawhan, S. D., D. A. Gurnett, D. L. Odem, R. A. Hoffman, and C. G. Park, The plasma wave and quasi-static electric field experiment (PWI) for Dynamics Explorer-A, *Space Sci. Instrum.*, *5*, 535, 1981.

Sonwalkar, V. S., R. A. Helliwell, and U. S. Inan, Wideband VLF electromagnetic bursts observed on the DE 1 satellite, *Geophys. Res. Lett.*, *17*, 1861, 1990.

Temerin, M. A., and D. Cravens, Production of electron conics by stochastic acceleration parallel to the magnetic field, *J. Geophys. Res.*, *95*, 4285, 1990.

Ungstrup, E., A. Bahnsen, H. K. Wong, M. Andre, and L. Matson, Energy source and generation mechanism for auroral kilometric radiation, *J. Geophys. Res.*, *95*, 5973, 1990.

Winglee, R. M., J. D. Menietti, and H. K. Wong, Numerical simulations of bursty radio emissions from planetary magnetospheres, *J. Geophys. Res.*, *97*, 17,131, 1992.

Winglee, R. M., and P. L. Pritchett, The generation of low-frequency electrostatic waves in association with auroral kilometric radiation, *J. Geophys. Res.*, *91*, 13,531, 1986.

Wong, H. K., and M. L. Goldstein, A mechanism for bursty radio emission in planetary magnetospheres, *Geophys. Res. Lett.*, *17*, 2229, 1990.

Wong, H. K., J. D. Menietti, C. S. Lin, and J. L. Burch, Generation of electron conical distributions by upper hybrid waves in the Earth's polar region, *J. Geophys. Res.*, *93*, 10,025, 1988.

Wu, C. S., Kinetic cyclotron and synchrotron maser instabilities: Radio emission processes by direct amplification of radiation, *Space Science Reviews*, *41*, 215, 1985.

Wu, C. S., and L. C. Lee, A theory of the terrestrial kilometric radiation, *Astrophys. J.*, *230*, 621, 1979.

Wu, C. S., H. K. Wong, D. J. Gorney, and L. C. Lee, Generation of the auroral kilometric radiation, *J. Geophys. Res.*, *87*, 4476, 1982.

J. L. Burch, Department of Space Sciences, Southwest Research Institute, San Antonio, TX 78228.

D. A. Gurnett and J. D. Menietti, Department of Physics and Astronomy, University of Iowa, Iowa City, IA 52242.

R. M. Winglee, Department of Geophysics, University of Washington, Seattle, WA 98195.

(Received June 24, 1992;
revised September 9, 1992;
accepted September 25, 1992.)